Bulletin of the Seismological Society of America, Vol. 86, No. 4, pp. 925–935, August 1996

The 25 March 1993 Scotts Mills, Oregon, Earthquake and Aftershock Sequence: Spatial Distribution, Focal Mechanisms, and the Mount Angel Fault

by G. C. Thomas, R. S. Crosson, D. L. Carver, and T. S. Yelin

Abstract The 25 March 1993 M_L = 5.7 crustal earthquake near Scotts Mills, Oregon, was the largest earthquake to occur in the Pacific Northwest in over a decade. The mainshock was located at 45.033° N, 122.586° W and at a depth of about 15.1 km, based on arrival time data from the short-period Pacific Northwest Seismograph Network. Beginning about 12 h after the mainshock, investigators from the U.S. Geological Survey deployed 22 digital seismographs to record aftershocks. Using data from the temporary and permanent stations, we analyzed a subset of 50 aftershocks with quality locations. Hypocenters of these aftershocks lie on a northwest-trending steeply dipping plane (strike 290 ± 10°, dipping 60 ± 5° to the north-northeast), in agreement with the preferred slip plane of the mainshock focal mechanism solution (strike 294°, dipping 58° to the north-northeast). The planar structure defined by the aftershock locations may be a southeast continuation of the Mount Angel Fault, a reverse fault identified from both surface and subsurface evidence. The mapped southeast extent of the Mount Angel Fault is located less than 10 km west of the Scotts Mills epicentral region. In addition, the mainshock focal mechanism solution, with a combination of reverse motion and right-lateral strike slip, has a geometry and sense of motion consistent with the Mount Angel Fault. While aftershock focal mechanisms are varied, *P* axes are consistently oriented in a subhorizontal north–south direction. This earthquake sequence, together with the geological and geophysical evidence for the Mount Angel Fault, suggests a significant crustal earthquake hazard for this region of northwest Oregon.

Introduction

The Scotts Mills mainshock occurred on 25 March 1993, at 5:34 a.m. PST (13:34 UT), with M_L = 5.7 and coda duration magnitude (M_D) = 5.6. This was the largest earthquake to occur in the Pacific Northwest since the M_L = 5.5 Elk Lake earthquake of 14 February 1981 (e.g., Grant *et al.*, 1984) and the M_L = 5.0 Goat Rocks earthquake of 28 May 1981 (Zollweg and Crosson, 1981). It has since been followed by the *M* 5.9 and *M* 6.0 earthquakes of 20 September 1993 near Klamath Falls in southern Oregon (e.g., Braunmiller *et al.*, 1995). Figure 1 shows the location of the Scotts Mills mainshock and other important crustal (North America plate) earthquakes in the Pacific Northwest. Using 93 *P*-phase arrivals recorded by the Pacific Northwest Seismograph Network (PNSN; described by Ludwin *et al.*, 1994), the Scotts Mills mainshock epicenter has been located at 45.033° N, 122.586° W with a focal depth of 15.1 km. Ground motion was felt in both the Willamette Valley and Puget Basin, from Roseburg, Oregon, to the south, to as far north as Seattle, Washington (Dewey *et al.*, 1994). Peak horizontal ground accelerations of 0.06 and 0.03 *g* were recorded at distances of 44 and 53 km, respectively (Dewey *et al.*, 1994). Madin *et al.* (1993) estimate the total property damage at over $28 million. No evidence of surface faulting was reported.

Historic seismicity in northwest Oregon has been concentrated in the northern Willamette Valley, between Salem and Portland (e.g., Ludwin *et al.*, 1991). Figure 2 shows a map of background seismicity for 1982–1992 for the Salem-Portland region. The Scotts Mills region, about 56 km south of Portland, is located near the southern boundary of seismic activity in western Oregon. Earthquakes in Portland have been interpreted to be related to one or more northwest-trending faults including the Portland Hills Fault (Yelin and Patton, 1991). Along the Portland Hills Fault, earthquakes with magnitudes as large as 3.5 have been observed to have focal mechanisms with a mixture of reverse and right-lateral strike-slip motion (Yelin, 1992). However, correlations of Portland earthquakes with individual faults is problematic

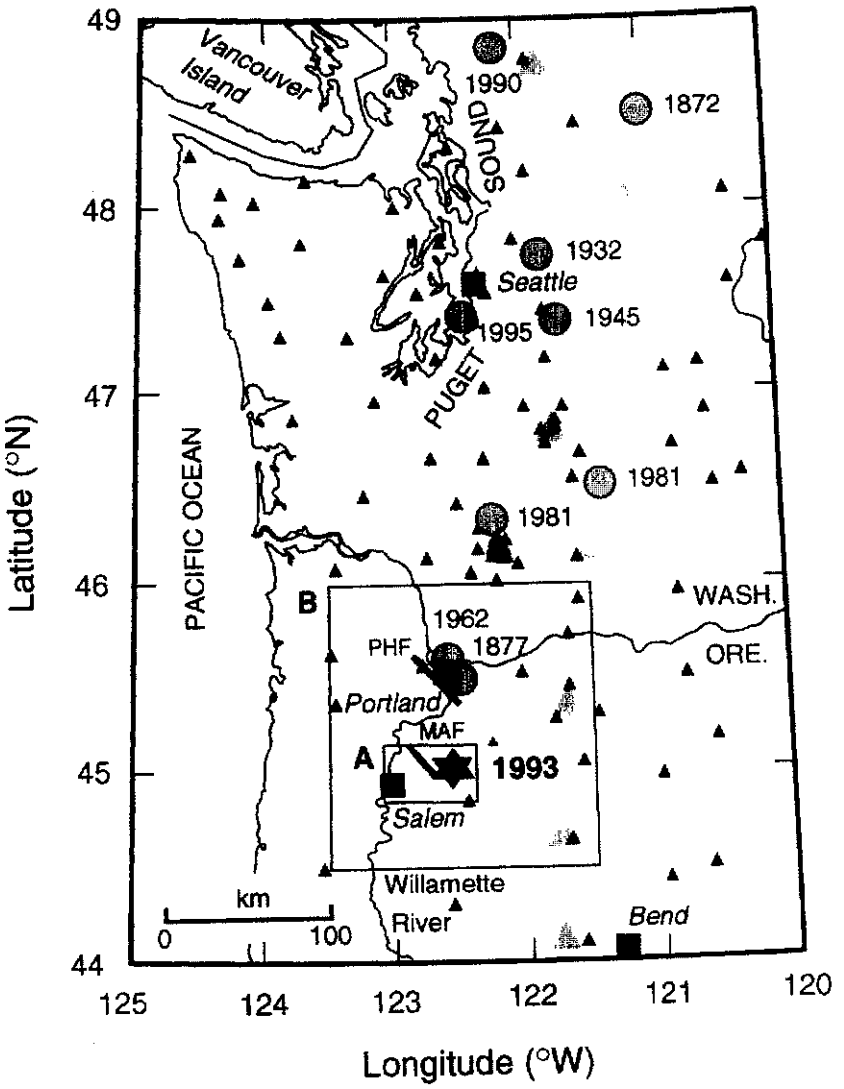

Figure 1. Map of western Washington and northwest Oregon featuring historic North America plate earthquakes of magnitude 5.0 or greater (circles), the Scotts Mills mainshock (star), PNSN seismographs operating in 1993 (solid triangles), and Quaternary volcanoes (gray triangles). PHF is the Portland Hills Fault, and MAF is the Mount Angel Fault. We refer to the area enclosed in box A as the Scotts Mills region, and the area enclosed in box B as the Salem–Portland region.

because the earthquakes are relatively deep (10–20 km) and the known faults lack evidence of recent surface displacement. Portland has experienced two moderate earthquakes: one of Modified Mercalli Intensity VII in 1877 (Thenhaus, 1978), and an M 5.2 in 1962 (Dehlinger *et al.*, 1963; Yelin and Patton, 1991).

There were no observed foreshocks to the Scotts Mills earthquake, but in 1990, several small ($M \approx 2$) earthquakes occurred approximately 20 km northwest of the Scotts Mills epicenter, near Woodburn, Oregon (see also Werner *et al.*, 1992). Figure 3 shows a map of epicenters of the Scotts Mills mainshock and 147 locatable aftershocks, as well as epicenters of earlier earthquakes including the Woodburn events of 1990. The Scotts Mills aftershock epicentral region is located about 10 km east of the most southeasterly mapped extent of the Mount Angel Fault.

The Mount Angel Fault (MAF) is part of the Gales Creek–Mount Angel lineament, a major northwest-trending structural zone that parallels the Portland Hills–Clackamas River structural zone (Beeson *et al.*, 1985, 1989) lying approximately 50 km to the north. The inferred surface trace of the MAF is shown in Figure 3. The MAF, with a mapped length of approximately 25 km, is primarily a subsurface reverse fault, dipping to the northeast (Werner *et al.*, 1992). Hampton (1972) first mapped the southeast portion of the fault based on vertical offsets of Miocene flows of the Columbia River Basalt group found in outcrops and water wells. Hampton's (1972) mapped northwest extent of the MAF was roughly midway between Woodburn and Mount Angel. Additional well studies and seismic reflection profiles indicate that the fault extends northwest, to approximately 4 km northwest of Woodburn (Werner *et al.*, 1992). The Miocene basalts have vertical displacements of up to 250 m, while the overlying Miocene and Pliocene fluvial and lacustrine sediments have offsets of approximately 100 m (Werner *et al.*, 1992). This differential offset suggests continuing post-Miocene displacement across the fault. The offsets and dips of individual flows in the Columbia River Basalt group,

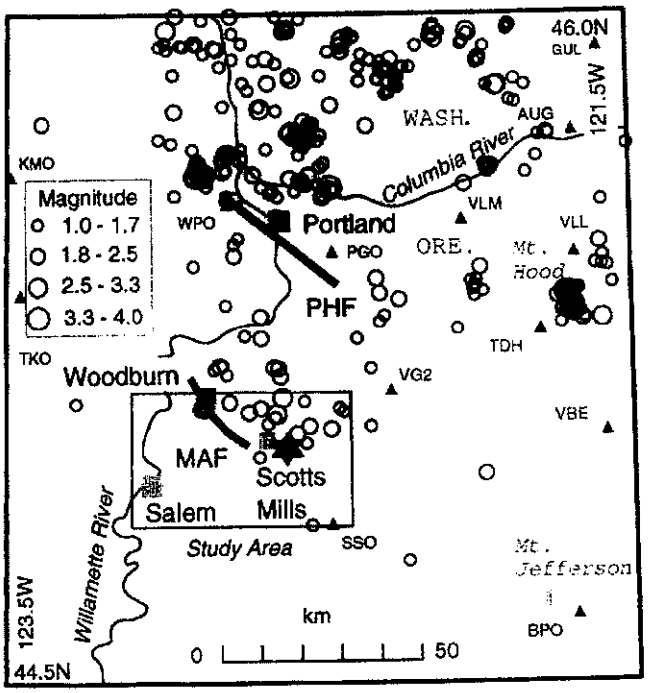

Figure 2. Background seismicity of the Salem–Portland region, 1982 through 1992. Labeled black triangles mark locations of PNSN seismographs operating in 1993, the star is the Scotts Mills mainshock epicenter, PHF indicates the Portland Hills Fault, MAF indicates the Mount Angel Fault, and gray triangles mark Quaternary volcanoes. Map border corresponds to box B in Figure 1.

together with focal mechanisms of the Woodburn earthquakes have led to the conclusion that the MAF is a result of both reverse motion and right-lateral strike-slip motion (Werner *et al.*, 1992).

Data and Instrumentation

The Scotts Mills earthquake sequence data set is a compilation of trace data collected by permanent short-period digital stations of the PNSN and by temporary digital stations installed by the U.S. Geological Survey (USGS). The Scotts Mills mainshock and initial 35 aftershocks were recorded only by the PNSN. Beginning about 12 h after the mainshock, investigators from the USGS installed temporary digital stations that collected data between 26 March and 15 April 1993 (Carver *et al.*, 1993). We first determined locations for a total of 148 earthquakes (Fig. 3), with 6 or more P arrivals and $M_D \geq 1.0$. In locating these events, we used data only from stations within 75 km epicentral distance. With the additional criteria of maximum azimuthal gap of 140°, and that travel times include both USGS and PNSN data, we selected a subset of 50 aftershocks, listed as events 2 through 51 in Table 1, for more detailed analysis. The average numbers of P picks and S picks per event are 31.5 and 5.6, respectively, and the S picks come exclusively from the USGS data.

The USGS temporary station deployment comprised a total of 30 sites in the Scotts Mills area (see Carver *et al.*, 1993), mostly within 10 km of the mainshock epicenter (Fig. 3). The two PNSN stations nearest the mainshock epicenter, SSO and VG2, were located at epicentral distances of 22 and 28 km, respectively (Fig. 2). Table 2 lists the pertinent station characteristics, and Table 3 summarizes the characteristics of the recording instruments. All USGS seismographs in the Scotts Mills area sampled data at 200 samples per second, and triggered recording durations were typically about 30 sec.

Data recorded on the temporary seismographs were formatted and archived by the Denver and Menlo Park offices of the USGS. We combined these data with PNSN data. Uncertainties in aftershock locations, initially determined using only PNSN data, were reduced by as much as a factor of 10 after the merging of the additional temporary station data. Preliminary analysis using only the PNSN data was inconclusive; thus, the results presented here depend critically on the combination of data.

Analysis

Methods

As our starting velocity model for aftershock locations, we chose the 1D layered model routinely used for the Puget Sound basin, model PS (Crosson, 1976), because the Willamette Valley is geologically similar to the Puget Sound basin. To determine an average V_P/V_S for the Scotts Mills area, we chose four moderate-sized events (numbers 8, 14, 15, and 47 in Table 1) and plotted the Wadati diagram, where S arrival times were determined only from horizontal-component data. This analysis could not be performed with larger aftershocks because the S arrival onsets were obscured by P codas. From this analysis, we found $V_P/V_S = 1.78$ (Poisson's ratio of 0.27). By contrast, the Puget Sound basin has a V_P/V_S of 1.73, where S arrivals are estimated primarily from vertical-component data. To construct our final velocity model, SM9, given in Table 4, we used the P velocities of the PS model and decreased S velocities so that $V_P/V_S = 1.78$.

To illustrate the difficulty in making S picks on vertical-component seismograms, we compare horizontal and vertical components from USGS station YOD with a seismogram from PNSN station SSO in Figure 4. Because of this difficulty, our analysis used only S arrival times picked on horizontal components of the temporary USGS stations. We note that our mainshock depth determination of 15.1 km, based only on PNSN P arrival times, is greater than the 12- to 13-km depth found by waveform inversion of regional broadband trace data (Nábelek and Xia, 1995). However, the lack of close-in stations that provide depth constraint makes the mainshock depth subject to greater uncertainty than the aftershocks.

Station travel-time corrections for USGS and PNSN sta-

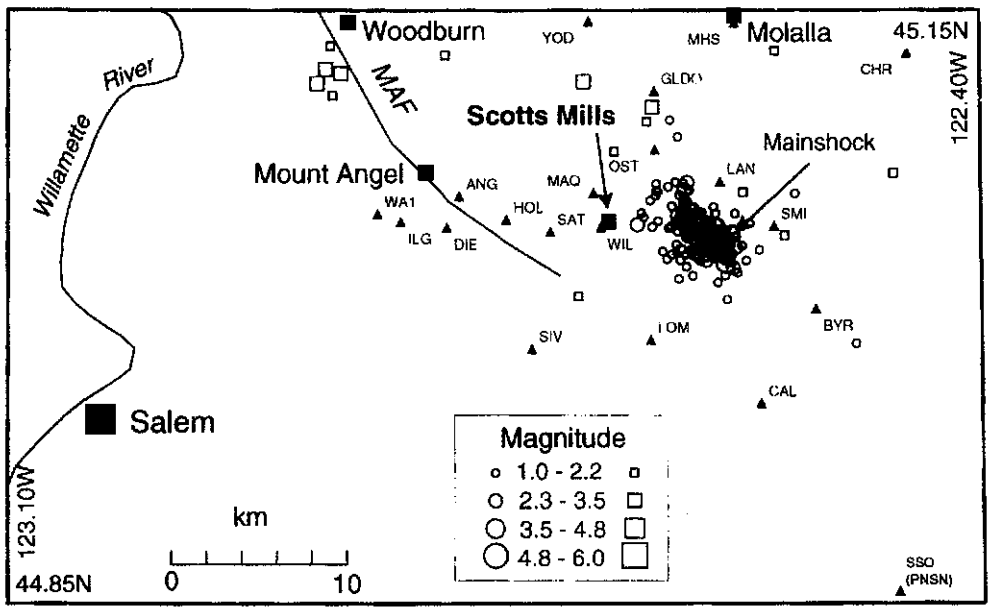

Figure 3. Map of Scotts Mills area. Triangles mark the locations of the USGS temporary seismograph stations and nearest PNSN station, SSO. Circles mark 148 epicenters of the Scotts Mills earthquake sequence through the end of July 1994, as determined in this study, and squares mark background seismicity for 1989 through February 1993, as listed in the PNSN catalog. MAF designates the Mount Angel Fault as inferred by Werner *et al.* (1992). Map boundary corresponds to box A in Figure 1.

tions were determined using a master event method. We chose two candidate events (14 and 15, in Table 1), based on a minimum of 15 *P* arrivals at temporary stations, and an azimuthal gap of less than 35°. We then investigated the hypocentral numerical variability of these two aftershocks in relationship to the other aftershocks, by applying the following jackknife-type analysis to each event.

For each earthquake, we started with a complete set of arrival times, deleted a random selection of 10% of the arrival times, and estimated the hypocenter using the starting velocity model PS. This process was repeated, generating 50 location estimates for each event. To quantify the spatial distributions of estimated locations, we formed, for each aftershock, a standard second moment, or "inertia," tensor (e.g., Arfken, 1985, pp. 217–218), assigning nondimensional unit "mass" to each estimated location. For each tensor, we found I_0, the root mean square (RMS) of the three principal moments (inertia tensor eigenvalues). For events 2 through 51 in Table 1, the I_0 values spanned two decades, ranging from about 0.01 km^2 to about 1 km^2. In particular, events 14 and 15 had I_0 values of 0.060 and 0.067 km^2, respectively. Approximately 70% of the events had larger values. Aftershocks with the smallest I_0 were interpreted as having the most stable locations.

Events 14 and 15 were then tested individually as master events. Station corrections were determined from each event, and the aftershocks were relocated. We found that RMS travel-time residuals, averaged over all aftershocks, equaled 0.16 sec for event 14 and 0.19 sec for event 15. Both values are smaller than the 0.24-sec average RMS residual for the PS model without station corrections and the 0.23-sec average RMS residual for model SM9 without station corrections. Finally, we selected event 14 as the best master event, and its travel-time residuals were used as station corrections for all aftershock locations.

Aftershock Locations

The mainshock and all aftershocks were relocated using the SM9 velocity model and the master event station corrections. Most aftershock depths fall in the depth range of 8 to 15 km. Although there is somewhat more scatter in depth for aftershocks prior to installation of the temporary stations, there does not appear to be a systematic bias in depth for aftershocks located only with data from PNSN stations. In performing waveform analysis of the 1990 Woodburn earthquakes, Werner *et al.* (1992) found focal depths in the 15- to 20-km range, while the PNSN catalog depths for the same earthquakes were around 30 km. Applying our location scheme to those same events gave focal depths around 17 km. From this, we infer that our model and station corrections provide quality locations for earthquakes in the Scotts Mills region, even when only PNSN data are available.

Figure 5 shows relocated epicenters of the subset of 50 aftershocks that have both USGS and PNSN data; the final locations are also listed in Table 1. The average of the formal standard errors in the vertical direction is 0.26 km. Figure 6 shows orthogonal cross sections of hypocenters of this subset of aftershocks, with projection planes striking north-

Table 1
Earthquake Locations*

Event	Date (Yr Mo Day)	Time (hr:min)	Latitude (°N)	Longitude (°W)	Depth (km)	M_D	Gap (°)	RMS residual (sec)
1	93 03 25	13:34	45.033	122.586	15.1	5.6	66	0.27
2	93 03 26	05:18	45.033	122.597	12.6	2.9	67	0.24
3	93 03 26	07:35	45.023	122.583	11.3	1.8	66	0.20
4	93 03 26	07:59	45.032	122.599	12.2	2.9	67	0.18
5	93 03 26	10:22	45.027	122.579	11.4	1.7	84	0.21
6	93 03 26	12:55	45.020	122.611	11.7	2.0	68	0.23
7	93 03 26	16:54	45.028	122.605	11.2	3.1	67	0.27
8	93 03 26	17:39	45.047	122.611	13.8	3.2	67	0.21
9	93 03 26	18:43	45.059	122.613	10.7	2.8	67	0.14
10	93 03 26	19:56	45.050	122.591	14.0	1.5	135	0.28
11	93 03 27	05:40	45.030	122.576	12.7	2.6	34	0.21
12	93 03 27	06:46	45.058	122.632	9.6	2.1	47	0.19
13	93 03 27	13:41	45.043	122.632	11.4	1.2	68	0.16
14	93 03 27	14:38	45.041	122.589	13.9	2.9	29	0.00
15	93 03 27	22:24	45.030	122.592	12.4	2.5	32	0.13
16	93 03 27	22:31	45.028	122.628	10.3	1.1	123	0.12
17	93 03 27	23:34	45.028	122.608	11.3	1.7	39	0.15
18	93 03 28	05:22	45.028	122.594	11.6	2.1	32	0.19
19	93 03 28	07:43	45.029	122.596	11.6	1.8	73	0.22
20	93 03 28	08:20	45.040	122.606	12.7	1.5	64	0.14
21	93 03 28	08:50	45.036	122.601	13.6	1.7	53	0.13
22	93 03 28	09:03	45.035	122.600	13.5	1.6	53	0.14
23	93 03 28	15:50	45.031	122.618	11.0	1.7	68	0.16
24	93 03 28	23:26	45.030	122.604	11.7	1.4	62	0.12
25	93 03 29	00:16	45.043	122.594	13.5	2.0	32	0.12
26	93 03 29	02:19	45.030	122.589	11.7	2.0	55	0.23
27	93 03 29	10:39	45.029	122.615	11.1	1.5	65	0.21
28	93 03 29	22:47	45.057	122.616	10.7	1.9	47	0.13
29	93 03 30	05:49	45.040	122.624	12.5	1.1	111	0.02
30	93 03 30	07:43	45.023	122.583	11.8	1.7	99	0.17
31	93 03 30	09:18	45.043	122.609	13.4	1.3	120	0.03
32	93 03 30	11:36	45.040	122.636	11.8	1.1	109	0.05
33	93 03 30	11:41	45.041	122.606	13.3	1.7	52	0.15
34	93 03 30	15:29	45.030	122.596	13.2	1.1	126	0.12
35	93 03 30	16:56	45.059	122.609	11.0	1.6	68	0.21
36	93 03 30	17:30	45.016	122.607	9.8	1.4	129	0.29
37	93 03 31	08:35	45.042	122.596	13.9	1.5	77	0.11
38	93 03 31	13:16	45.024	122.616	10.6	1.4	136	0.08
39	93 03 31	19:28	45.042	122.593	13.6	1.8	96	0.26
40	93 03 31	23:43	45.042	122.611	12.8	1.0	69	0.06
41	93 04 01	04:13	45.023	122.582	11.2	1.3	112	0.04
42	93 04 01	04:35	45.037	122.587	13.0	1.2	130	0.05
43	93 04 01	05:10	45.023	122.580	11.4	1.1	66	0.04
44	93 04 01	09:37	45.025	122.583	11.2	1.1	62	0.03
45	93 04 01	09:39	45.038	122.590	12.9	1.2	79	0.07
46	93 04 05	06:38	45.019	122.579	12.0	2.2	132	0.18
47	93 04 06	09:47	45.042	122.646	11.6	2.6	79	0.16
48	93 04 07	04:32	45.043	122.615	14.3	2.5	67	0.26
49	93 04 07	20:51	45.045	122.642	12.6	2.2	78	0.25
50	93 04 08	06:24	45.038	122.618	13.2	2.3	106	0.32
51	93 04 15	06:44	45.017	122.575	13.4	2.2	82	0.33
a	93 03 25	14:20	45.027	122.586	12.5	3.1	66	0.27
b	93 03 25	15:35	45.028	122.589	13.4	3.2	66	0.28
c	93 06 08	00:01	45.022	122.583	13.9	3.9	66	0.33
d	93 04 30	23:01	45.042	122.596	14.9	2.5	66	0.10

*Event 1 is the mainshock; events 2 through 51 are the subset of aftershocks that combine USGS and PNSN data; and events *a* through *d* are additiona aftershocks with focal mechanisms shown in Figure 7, but located only with PNSN data.

Table 2
Locations of USGS Temporary Stations and Two Closest PNSN Stations

Station Name	Recorder Type	North Latitude (deg. min. sec.)	West Longitude (deg. min. sec.)	Elevation (km)	Date Installed*	Date Removed
ANG	GEOS	45 03 22.14	122 46 29.70	0.128	3/30	4/14
BC1	Reftek	45 01 44.10	122 37 04.80	0.192	3/27	4/01
BYR	DR-200	44 59 56.40	122 31 07.32	0.660	3/28	4/01
BYR	GEOS	44 59 56.40	122 31 07.32	0.660	4/01	4/15
CAL	DR-200	44 57 03.80	122 33 29.20	0.615	3/26	4/01
CAL	GEOS	44 57 03.80	122 33 29.20	0.615	4/01	4/14
CHR	GEOS	45 07 42.20	122 27 06.90	0.349	3/27	3/30
DIE	DR-200	45 02 25.08	122 47 01.70	0.064	3/27	4/01
GLDO	GEOS	45 06 33.00	122 38 02.00	0.091	3/26	3/29
HA1	Reftek	45 30 00.00	122 39 00.00	0.018	3/23	3/28
HOL	DR-200	45 02 39.12	122 44 26.40	0.092	3/27	4/01
ILG	DR-200	45 02 35.40	122 49 00.50	0.052	3/27	3/28
LAN	DR-200	45 03 48.80	122 35 12.48	0.207	3/26	4/01
LOM	DR-200	44 59 00.60	122 38 14.40	0.277	3/26	4/01
MAQ	GEOS	45 03 27.60	122 40 41.40	0.116	3/27	3/30
MHS	GEOS	45 08 37.80	122 34 32.90	0.117	3/27	3/30
OST	DR-200	45 04 46.80	122 38 01.10	0.159	3/26	4/01
OST	GEOS	45 04 46.80	122 38 01.10	0.159	3/31	4/11
SAT	DR-200	45 02 17.10	122 42 33.50	0.181	3/27	4/01
SIV	GEOS	44 58 44.40	122 43 22.75	0.308	3/27	4/14
SMI	DR-200	45 02 27.30	122 32 53.52	0.415	3/26	4/01
SMI	GEOS	45 02 27.30	122 32 53.52	0.415	3/31	4/14
SSO	PNSN	44 51 21.60	122 27 37.80	1.242	9/91	—
VG2	PNSN	45 09 20.00	122 16 15.00	0.823	9/85	—
WA1	Reftek	45 02 49.58	122 50 00.53	0.056	3/27	4/01
WB1	Reftek	45 02 49.62	122 50 09.46	0.056	3/27	4/01
WC1	Reftek	45 02 43.99	122 50 04.98	0.055	3/27	4/01
WIL	DR-200	45 02 24.60	122 40 23.10	0.216	3/27	3/29
YOD	GEOS	45 08 40.50	122 40 51.75	0.067	3/27	3/30

*Installation and removal dates are given in month/day of 1993, except the PNSN stations, where the installation dates are listed in month/year.

Table 3
Summary of Digital Seismograph Parameters

Recorder Type	Deployment Group	Number of Channels*	Sensor*	Sensor Natural Frequency, f_0 (Hz)	Sample Rate (Samples/sec)	Dynamic Range (bits)
GEOS	Menlo Park	3/3	L-22/FBA	2.0/80.0*	200.0	16
DR-200	Denver	3/0	S-6000†	2.1/1.7‡	200.0	16
Reftek§	Golden	3/3	L-22/FBA	2.0/50.0*	200.0	16
PNSN	PNSN	1/0	L-4C or S-13	1.0	101.016	14

*Velocity/acceleration.
†Except station BYR with an L-22 sensor.
‡Vertical/horizontal components, except station BYR, which had $f_0 = 2.0$ for all components.
§Stations BC1 and HA1 had six acceleration channels with $f_0 = 50.0$ Hz, and station HA1 had a sample rate of 100 samples/sec.

northeast and east-southeast. The cross sections show a steeply dipping planar structure with strike 290 ± 10° and dipping 60 ± 5° to the north-northeast, determined by visual inspection. We refer to this planar structure as the Scotts Mills Seismic Zone (SMZ) and interpret it as a subsurface oblique reverse fault. Hypocenters of four events in Figure 6 are well removed from the SMZ and may lie on an auxiliary fault or faults. The observed planar structure does not appear to be an artifact of station geometry or location method. It has persisted through several relocation schemes with several different velocity models as well as various station corrections (including zero station corrections). However, to further test for the possibility that hypocenter uncertainty may contribute to the apparent alignment, we repeated the previously described jackknife analysis on the relocated events (2 through 51 in Table 1) using our final model and

Table 4
Model SM9

Depth (km)	V_P (km/sec)	V_S (km/sec)
0.0	5.36	3.01
10.0	6.61	3.71
16.0	6.70	3.76
22.0	6.91	3.88
32.0	7.11	3.99
35.0	7.16	4.02
38.0	6.87	3.86
41.0	7.75	4.35

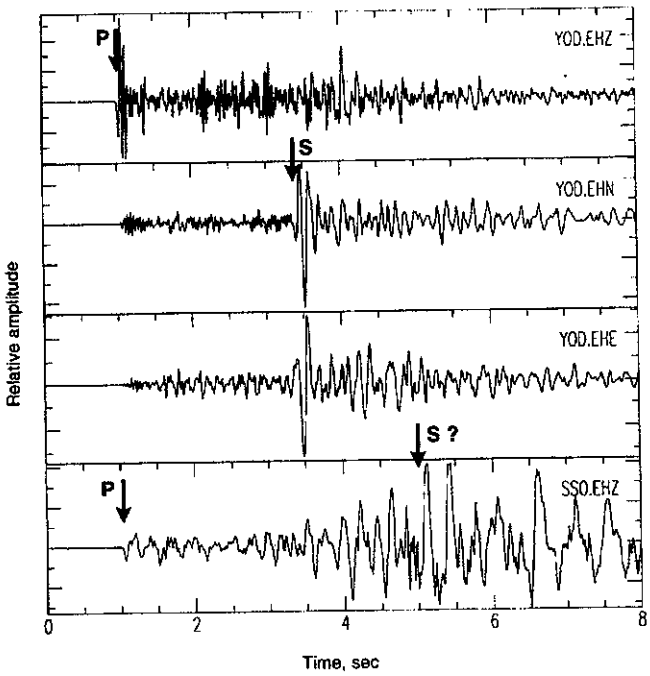

Figure 4. Unfiltered velocity seismograms for event 12. The top three traces are the high gain vertical, north, and east components, respectively, of USGS station YOD (10.4 km epicentral distance), and the bottom trace is PNSN station SSO (26.2 km epicentral distance). Traces are aligned on the *P* arrival.

station corrections. The results did not show preferential location dispersion alignment along the SMZ. Also, using standard-error ellipse analysis, we found that the major axes of the error ellipses were not preferentially aligned in the plane of the aftershock distribution.

Focal Mechanisms

Using *P*-wave first motions and the layered velocity model SM9, we fit double-couple focal mechanism solutions to the mainshock and 10 aftershocks. Mechanisms for six of the aftershocks utilize both USGS and PNSN data; the mainshock and four aftershocks (events *a* through *d* in Table 1) utilize PNSN data only. Lower-hemisphere equal-angle projections are plotted in Figure 7.

The focal mechanism solution from *P*-wave first motions agrees well with the solution determined by waveform inversion of regional broadband data (Nábelek and Xia, 1995) and waveform inversion of teleseismic data (Nábelek and Xia, 1995; Dewey *et al.*, 1994). The northwest-trending nodal plane for the mainshock solution, strike 294° and dip of 58° to the north-northeast, has a geometry similar to the planar structure of the aftershock distribution. We infer that this northwest-striking nodal plane is the slip plane of Scotts Mills mainshock. With a rake of 138°, the motion on this slip plane is oblique thrust, with approximately a 1:1 ratio of strike slip to reverse motion.

Focal mechanisms for the aftershocks (Fig. 7) exhibit significant variability, ranging from nearly pure strike slip to nearly pure reverse motion. The largest aftershocks in the sequence (events 8 and *a* through *d*, in Table 1) have solutions generally similar to the mainshock (right-lateral strike slip with a smaller component of reverse motion). The largest aftershock of the entire Scotts Mills sequence (event *c* M_D = 3.9), occurring on 8 June 1993, has a solution quite similar to the first located aftershock (event *a*, M_D = 3.1), that occurred 1 hr after the mainshock. Events *a* and *c* both have solutions with northwest-trending nodal planes, striking 336° and 333°, respectively, and dipping 63° and 44° respectively, to the northeast.

While the focal mechanisms vary, the *P* axes and inferred directions of maximum stress are quite consistent. A combined *P* and *T* axis distribution, shown in the inset of Figure 7, shows that *P* axes tend to horizontal and clustered about a north–south direction. This is in excellent agreement with an approximate N10°E direction of maximum horizontal compressive stress as determined by borehole breakouts in both northwest Oregon (Werner *et al.*, 1991), and Puget Sound, Washington (Magee and Zoback, 1992), but is rotated substantially from the N50°E direction of convergence between the Juan de Fuca and North America plates (e.g. Riddihough, 1984). The north–south orientation of *P* axes is also consistent with focal mechanism studies of crustal earthquakes in western Washington (e.g., Ma *et al.*, 1991; Crosson, 1972, 1983), eastern Washington (Malone *et al.*, 1975), and Vancouver Island (Rogers, 1979). A tectonic model for the Pacific Northwest that adequately relates the oblique oceanic-continental convergence to the observed north–south regional compressive stress is a subject of continuing research.

Frequency-Magnitude Relations

Magnitude calculations were made using the coda duration scheme of Crosson (1972), modified to use the median rather than the mean duration. Durations were measured from the *P* onset to a time where the signal level was twice the presignal noise level. Durations were chosen only on USGS stations HOL, LAN, OST, and WIL (Table 2), and PNSN stations BPO, FBO, MTM, TKO, VBE, and VLM (Ludwin *et al.*, 1994), all within 75 km epicentral distance. Mainshock durations could not be measured from digital data because the PNSN data were truncated. Instead, durations were de

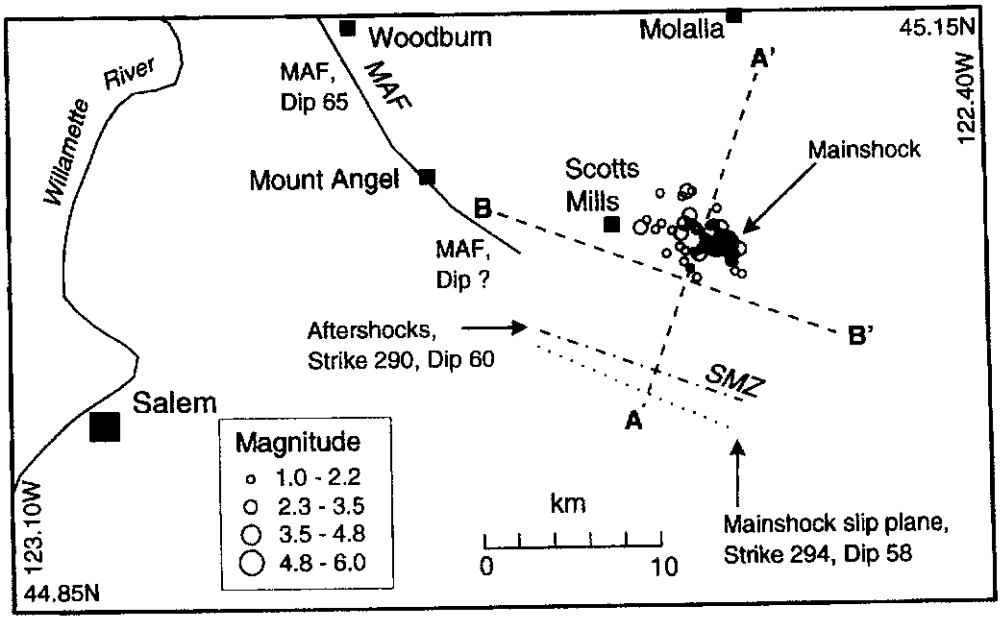

Figure 5. Circles mark epicenters of a subset of 50 events for which we are able to combine USGS and PNSN data. Dashed lines A-A′ and B-B′ correspond to projection planes of the cross sections in Figure 6. Dash-dot line (designated SMZ) and the dotted line are surface projections of the planar structure in the aftershock spatial distribution and the mainshock focal mechanism preferred slip plane, respectively.

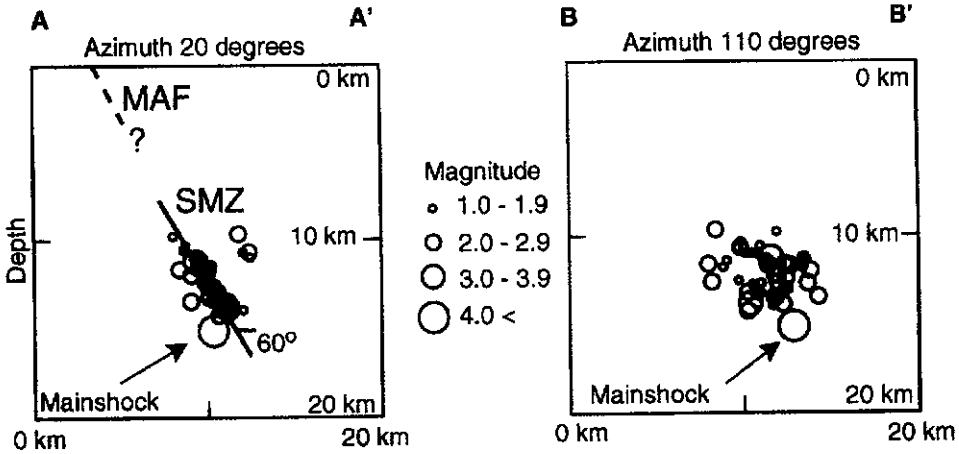

Figure 6. Orthogonal cross sections of earthquakes shown in Figure 5. In section A-A′, we find that 46 of the 50 earthquakes appear to form a steeply dipping planar structure (SMZ). Four outlier events are located to the north (right) of the general trend. The dashed line marks the projection of the MAF. Section B-B′ shows that the mainshock occurred at the deepest part of the SMZ. Point A is located at 44.95° N, 122.65° W, and point B is located at 45.05° N, 122.75° W.

termined from analog records of four PNSN stations. The local Richter magnitude estimate for the mainshock is based on amplitudes recorded by horizontal-component digital PNSN stations (SEE and SEN) with simulated Wood-Anderson responses.

Cumulative frequency-magnitude data for the earthquake sequence through the end of 1993 (132 earthquakes) are plotted in Figure 8. There is a linear trend in the plot for aftershocks in the range $1.7 < M_D < 3.3$ that conforms to the standard Gutenberg-Richter relation,

$$\log(N) = a - bM,$$

where N is the number of earthquakes with magnitude

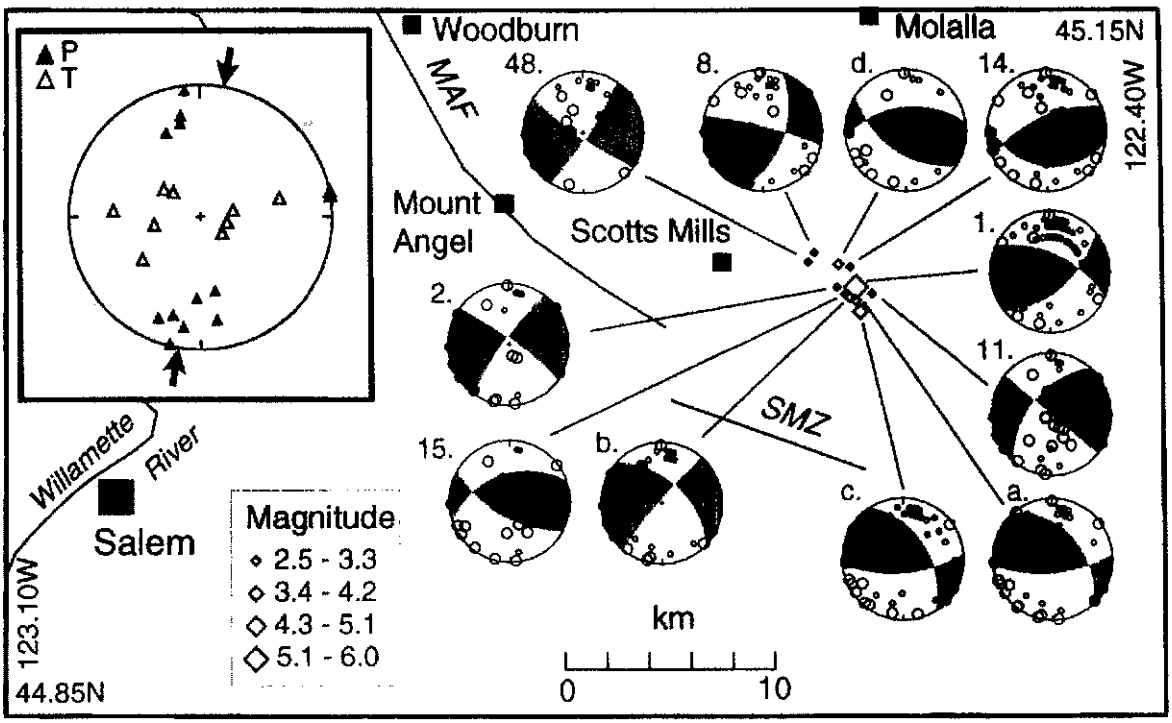

Figure 7. Map of epicenters and corresponding focal mechanisms. Filled diamonds mark epicenters of events for which mechanisms were fit to USGS and PNSN data while open diamonds were fit to PNSN data only. Focal mechanisms are plotted as lower-hemisphere equal-angle projections. Within each focal mechanism, filled circles represent compressional first motion, and open circles are dilatational. Larger circles correspond to rays that travel through the upper hemisphere. The inset shows the composite projection of P and T axes for all 11 focal mechanism solutions. Filled triangles are P axes, and hollow triangles are T axes. The dark arrows indicate the N10° E direction of maximum horizontal compressive stress in northwest Oregon found from borehole studies (Werner *et al.*, 1991), and the gray arrows indicate the N50°E direction of convergence between the subducting Juan de Fuca plate and overriding North America plate (e.g., Riddihough, 1984).

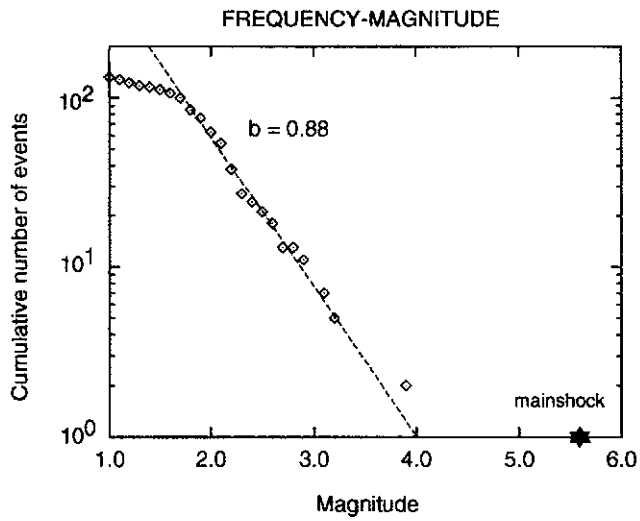

Figure 8. Magnitude-frequency plot for the Scotts Mills earthquake sequence for events from 25 March through 31 December, 1993.

greater than M, and a and b are constants. For $M_D < 1.7$, the departure from the linear trend is interpreted as an indication of a threshold magnitude of about 1.7 for reliable detection by the PNSN in the Scotts Mills area. The threshold magnitude of about 1.7 is also observed in similar plots with time windows that exclude the USGS data. For the Scotts Mills aftershock sequence through the end of 1993, we find $b = 0.88 \pm 0.16$, determined by the method of maximum likelihood estimation discussed in Shi and Bolt (1982), with a threshold magnitude of 1.7. The large uncertainties are the result of a relatively small total number of events (100 of magnitude 1.7 or larger). A curve with this slope is plotted as a dashed line in Figure 8.

The b value of 0.88 for the Scotts Mills aftershock sequence is slightly greater than b values for other aftershock sequences in the Pacific Northwest, such as 0.77 ± 0.05 for the Elk Lake aftershock sequence of 1981 (Grant *et al.* 1984) and 0.67 ± 0.01 for the posteruptive Mt. St. Helens sequence of 1980 (Weaver *et al.*, 1981). However, the above values are smaller than the b value of 1.02 for Puget Sound

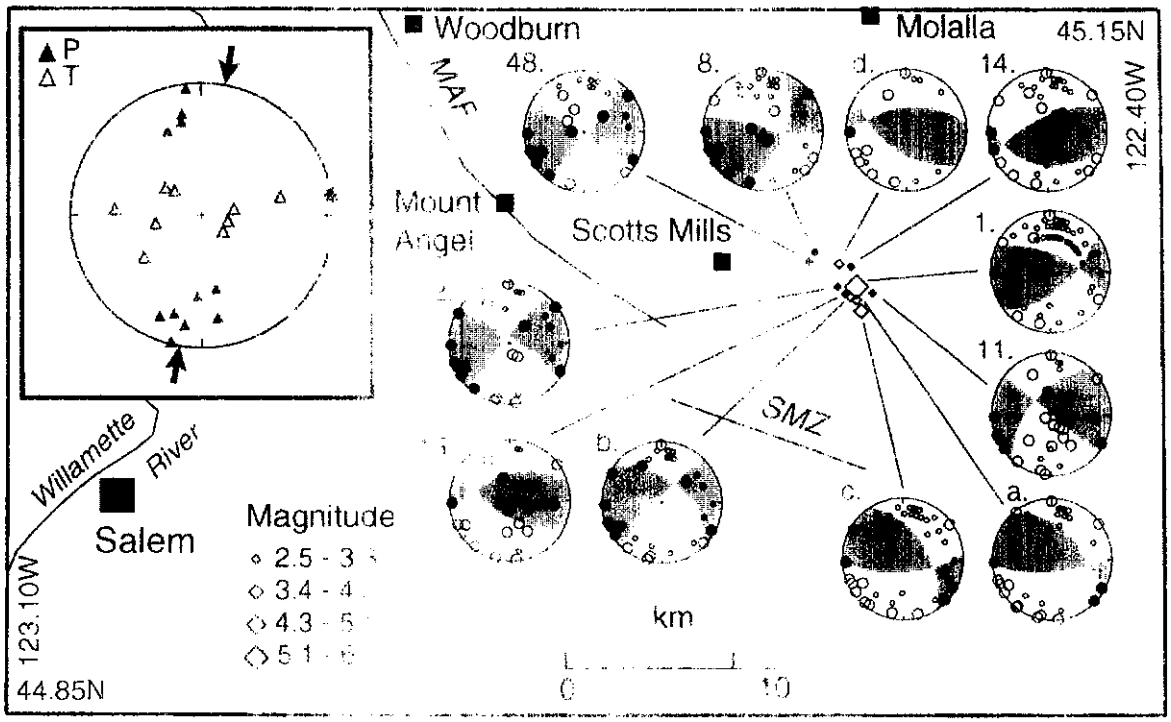

Figure 7. Map of epicenters and corresponding focal mechanisms. Filled diamonds mark epicenters of events for which mechanisms were fit to USGS and PNSN data while open diamonds were fit to PNSN data only. Focal mechanisms are plotted as lower-hemisphere equal-angle projections. Within each focal mechanism, filled circles represent compression first motion, and open circles are dilatational. Larger circles correspond to rays that travel through the upper hemisphere. The inset shows the composite projection of *P* and *T* axes for all 11 focal mechanism solutions. Filled triangles are *P* axes, and hollow triangles are *T* axes. The dark arrows indicate the N10° E direction of maximum horizontal compressive stress in northwest Oregon found from borehole studies (Werner [illegible] 1991), and the gray arrows indicate the N50 E direction of convergence between the subducting Juan de Fuca plate and overriding North America plate (e.g., Riddihough [illegible] 1984).

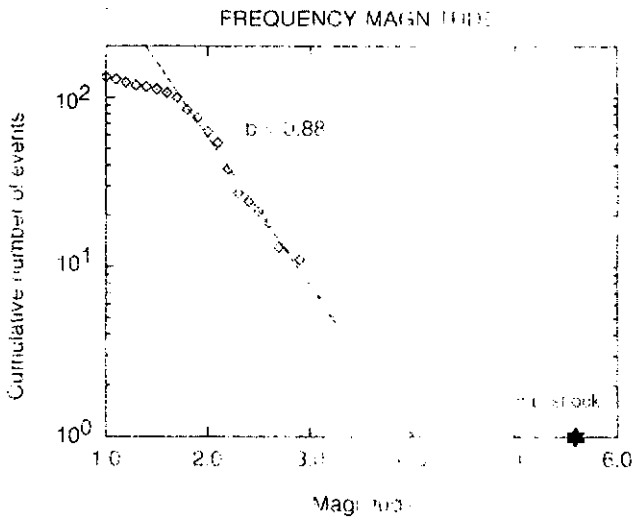

Figure 8. Magnitude frequency plot for the Scotts Mills earthquake sequence for events from 25 March through 31 December, 1993.

greater than M_t, and a and b are constants. For $M_t < 1.7$, the departure from the linear trend is interpreted as an indication of a threshold magnitude of about 1.7 for reliable detection by the PNSN in the Scotts Mills area. The threshold magnitude of about 1.5 is also observed in similar plots with time windows that exclude the USGS data. For the Scotts Mills aftershock sequence through the end of 1993, we find $b = 0.88 \pm 0.16$, determined by the method of maximum likelihood estimation discussed in Shi and Bolt (1982), with a threshold magnitude of 1.7. The large uncertainties are the result of a relatively small total number of events (100 of magnitude 1.7 or larger). A curve with this slope is plotted as a dashed line in Figure 8.

The b value of 0.88 for the Scotts Mills aftershock sequence is slightly greater than b values for other aftershock sequences in the Pacific Northwest, such as 0.77 ± 0.05 for the Elk Lake aftershock sequence of 1981 (Grant *et al.*, 1984) and 0.67 ± 0.01 for the posteruptive Mt. St. Helens sequence of 1980 (Weaver *et al.*, 1981). However, the above values are smaller than the b value of 1.02 for Puget Sound

crustal (North America plate) earthquakes for 1970 through 1978 (Crosson, 1983).

Discussion

The mainshock and aftershocks occurred in the mid-crust of the North America plate, between 8 and 15 km in depth, with epicenters near the boundary between the Willamette Valley and the Cascade Range. We conclude from our analysis of aftershocks that the mainshock ruptured on a plane, the SMZ, with a strike of 290 ± 10°, and a dip of 60 ± 5° to the north-northeast. The area of the rupture surface, as inferred from the aftershock distribution, was about 28 km^2 (Fig. 6, section B-B′). This value is consistent with the mainshock rupture area estimated by Nábelek and Xia (1995), based on a source time estimation from regional broadband data.

The preferred slip plane for the mainshock focal mechanism has a geometry and sense of motion generally consistent with the Mount Angel Fault (Fig. 7). The mainshock fault-plane solution from first-motion observations strikes 294° and dips 58° to the north-northeast; this agrees with the aftershock distribution. In comparison, the southeast portion of the MAF has a mapped strike of 305° (Werner *et al.*, 1992). Although the dip of the southeast section of the MAF is poorly constrained, the northwest part of the MAF has a dip of 65° to the northeast, based on a single seismic reflection line 2 km southeast of Woodburn (Werner *et al.*, 1992). The sense of motion of the Scotts Mills mainshock and several aftershocks, a combination of reverse and right-lateral strike-slip motion, is consistent with interpretations of post-Miocene displacement on the southeast section of the MAF. The strike of the MAF apparently changes as it enters the Willamette Valley, as shown in Figure 7. The northwest portion of the MAF, near Woodburn, has a mapped strike of 330°. In addition, Werner *et al.* (1992) determined a composite focal mechanism for the 1990 Woodburn earthquakes and for those earthquakes inferred right-lateral motion on a plane striking 350 ± 10°. This value is significantly different from the trend of the southeast portion of the MAF and the strike of the Scotts Mills mainshock slip plane.

We propose two alternative structural models for the relationship between the MAF and the SMZ. In the first model, the "fault zone model," the MAF is a zone consisting of several discrete faults. In this model, the MAF "zone" has a length of at least 25 km, and the fault strikes range from 290°, in the Cascade foothills, to up to 350° in the Willamette Valley near Woodburn. In this model, the Scotts Mills earthquake and aftershocks occurred on one fault within the zone. We note that Werner *et al.* (1992) interpret the northwest portion of the MAF as consisting of several faults, based on a seismic reflection line through Woodburn. An alternative model, the "listric model," is that the MAF is a single but curved fault. The dip decreases with depth and the strike becomes more westerly toward the southeast end of the fault. In this model, the Scotts Mills earthquake occurred on the southeastern end of the MAF. Both of these models are consistent with the surface projections of the MAF and SMZ shown in Figure 7. Examples of more complex models for the MAF are described by Werner *et al.* (1992).

The 1990 Woodburn earthquakes and the 1993 Scotts Mills sequence are evidence that the MAF is a seismically active structure. It may be an old shear zone reactivated by current north–south compressive stress. There is no compelling reason to exclude the possibility of a magnitude 6, or larger, earthquake occurring anywhere on the MAF, including the northwest portion near populated areas of the Willamette Valley. Indeed, as a hypothetical example, we can estimate the size of an earthquake rupturing through the entire seismogenic thickness in this region, inferring the thickness from the maximum depth of the Scotts Mills aftershocks. Thus, if we assume that a portion of the MAF could rupture over a circular zone from about 16 km in depth to the surface (18-km distance along a 60° dipping plane) and also assume a stress drop of 40 bars, then the Brune (1970, 1971) relation,

$$M_0 = \frac{16r^3\Delta\sigma}{7},$$

gives a moment estimate of 6.7 × 10^{25} dyne-cm, corresponding to an M_w = 6.5 earthquake.

Conclusion

Aftershocks of the Scotts Mills earthquake align on a plane striking 290° and dipping 60° to the north-northeast. The mainshock focal mechanism is consistent with oblique thrust on this plane, driven by north–south tectonic stress. Comparison of the rupture surface with the orientation and position of the Mount Angel Fault suggests a close connection between the Scotts Mills earthquake and the MAF. Two alternatives are (a) the Scotts Mills earthquake occurred on a subsidiary fault within a complex fault zone comprising the MAF, or (b) the Scotts Mills earthquake lies on a deep southeast extension of a curved MAF, which exhibits listric geometry at depth.

The combination of near-surface geologic and geophysical evidence of faulting and a significant earthquake at mid-crustal depth of 15 km suggests that the MAF, and perhaps other crustal faults in the Pacific Northwest, may be seismogenic through approximately half the thickness of the crust. Therefore, the seismic hazard posed by the MAF, or related faults, may be higher than previously estimated. The MAF may indicate a dominant style of faulting, activated or reactivated by north–south tectonic stress, that could apply to the Portland Hills Fault as well as other faults of a similar nature in this region.

Data Availability

The Scotts Mills digital data set (~250 Mb) is available upon request. This includes trace data and arrival time data recorded by USGS and PNSN seismographs.

Acknowledgments

This analysis would not have been possible without the data collection by T. Bice, T. MacDonald, M. Meremonte, R. Norris, D. Overturf, E. Sembera, and D. Worley, all of the USGS, and the data processing by Gary Glassmoyer, also of the USGS. The authors gratefully acknowledge the critical manuscript reviews by Jim Zollweg, Chris Stephens, and Jerry Eaton. This work was supported by USGS Project Numbers 14-34-92-A0963 and 14-08-0001-G1803. One of us (G.C.T.) was additionally partially supported by an ARCS Fellowship.

References

Arfken, G. (1985). *Mathematical Methods for Physicists*, Academic Press, Inc., San Diego, California, 985 pp.

Beeson, M. H., K. R. Fecht, S. P. Reidel, and T. L. Tolan (1985). Regional correlations within the Frenchman Springs Member of the Columbia River Basalt Group: new insights into the middle Miocene tectonics of northwestern Oregon, *Oregon Geol.* **47,** 87–96 (published by the Oregon Department of Geology and Mineral Industries).

Beeson, M. H., T. L. Tolan, and J. L. Anderson (1989). The Columbia River Basalt Group in Western Oregon: geologic structures and other factors that controlled the flow emplacement patterns, in *Volcanism and Tectonism in the Columbia River Flood-Basalt Province*, S. P. Reidel and P. R. Hooper (Editors), *Geol. Soc. Am. Spec. Pap.* **239,** 233–246.

Braunmiller, J., J. Nábelek, B. Leitner, and T. Qamar (1995). The 1993 Klamath Falls, Oregon, earthquake sequence: source mechanisms from regional data, *Geophys. Res. Lett.* **22,** 105–108.

Brune, J. N. (1970). Tectonic stress and the spectra of seismic shear waves from earthquakes, *J. Geophys. Res.* **75,** 4997–5009.

Brune, J. N. (1971). Tectonic stress and the spectra of seismic shear waves from earthquakes: corrections, *J. Geophys. Res.* **76,** 5002.

Carver, D., D. Worley, and T. Yelin (1993). Digital recordings of the March 25, 1993, Scotts Mills, Oregon earthquake, *U.S. Geol. Surv. Open-File Rept. 93-535.*

Crosson, R. S. (1972). Small earthquakes, structure, and tectonics of the Puget Sound region, *Bull. Seism. Soc. Am.* **62,** 1133–1171.

Crosson, R. S. (1976). Crustal structure modeling of earthquake data 2. Velocity structure of the Puget Sound Region, Washington, *J. Geophys. Res.* **81,** 3047–3054.

Crosson, R. S. (1983). Review of Seismicity in the Puget Sound region from 1970 through 1978, in *Proc. of Workshop XIV, Earthquake Hazards of the Puget Sound Region, Washington, U.S. Geol. Surv. Open-File Rept. 83-19,* 6–18.

Dehlinger, P., R. G. Bowen, E. F. Chiburis, and W. H. Westphal (1963). Investigations of the earthquake of November 5, 1962, north of Portland, *The Ore Bin* **25,** 53–68.

Dewey, J. W., B. G. Reagor, D. Johnson, G. L. Choy, and F. Baldwin (1994). The Scotts Mills, Oregon, earthquake of March 25, 1993: intensities, strong-motion data, and teleseismic data, *U.S. Geol. Surv. Open-File Rept. 94-163.*

Grant, W. C., C. S. Weaver, and J. E. Zollweg (1984). The 14 February 1981 Elk Lake, Washington, earthquake sequence, *Bull. Seism. Soc. Am.* **74,** 1289–1309.

Hampton, E. R. (1972). Geology and ground water of the Molalla-Salem slope area, northern Willamette Valley, Oregon, *U.S. Geol. Surv. Water Supply Pap. 1997.*

Ludwin, R. S., A. I. Qamar, S. D. Malone, C. Jonientz-Trisler, R. S. Crosson, R. Benson, and S. C. Moran (1994). Earthquake Hypocenters in Washington and Northern Oregon, 1987–1989, and Operation of the Washington Regional Seismograph Network, *Washington Division of Geology and Earth Resources Information Circular 89,* 40 pp. (published by the Washington State Department of Natural Resources).

Ludwin, R. S., C. S. Weaver, and R. S. Crosson (1991). Seismicity of Washington and Oregon, in *Neotectonics of North America, Decade Map Volume 1*, D. B. Slemmons, E. R. Engdahl, M. D. Zoback, and D. D. Blackwell (Editors), 77–97.

Ma, L., R. S. Crosson, and R. S. Ludwin (1991). Focal mechanisms of western Washington earthquakes and their relationship to regional tectonic stress, *U.S. Geol. Surv. Open-File Rept. 91-441-D.*

Madin, I., G. Priest, M. Mabey, S. Malone, T. Yelin, and D. Meier (1993). March 25, 1993 Scotts Mills earthquake—western Oregon's wake-up call, *Oregon Geol.* **55,** 51–56 (published by the Oregon Department of Geology and Mineral Industries).

Magee, M. and M. L. Zoback. (1992). Wellbore breakout analysis for determining tectonic stress orientations in Washington State, *U.S. Geol. Surv. Open-File Rept. 92-715.*

Malone, S. D., G. H. Rothe, and S. W. Smith (1975). Details of earthquake swarms in the Columbia Basin, Washington, *Bull. Seism. Soc. Am.* **65,** 855–864.

Nábelek, J. and G. Xia (1995). Moment-tensor analysis using regional data: application to the 25 March, 1993, Scotts Mills, Oregon, Earthquake, *Geophys. Res. Lett.* **22,** 13–16.

Riddihough, R. (1984). Recent movements of the Juan de Fuca Plate System, *J. Geophys. Res.* **89,** 6980–6994.

Rogers, G. C. (1979). Earthquake fault plane solutions near Vancouver Island, *Can. J. Earth Sci.* **16,** 523–531.

Shi, Y. and B. A. Bolt (1982). The standard error of the magnitude-frequency *b*-value, *Bull. Seism. Soc. Am.* **72,** 1677–1687.

Thenhaus, P. C. (1978). A study of the October 12, 1877 Oregon earthquakes, *U.S. Geol. Surv. Open-File Rept. 78-234.*

Weaver, C. S., W. C. Grant, S. D. Malone, and E. T. Endo (1981). Post-May 18 seismicity: volcanic and tectonic implications, *U.S. Geol. Surv. Profess. Pap. 1250,* 109–121.

Werner, K. S., E. P. Graven, T. A. Berkman, and M. J. Parker (1991). Direction of maximum horizontal compression in western Oregon determined by borehole breakouts, *Tectonics* **10,** 948–958.

Werner, K., J. Nábelek, R. Yeats, and S. Malone (1992). The Mt. Angel Fault: implications of seismic-reflection data and the Woodburn, Oregon, earthquake sequence of August, 1990, *Oregon Geol.* **54,** 112–117 (published by the Oregon Department of Geology and Mineral Industries).

Yelin, T. and H. Patton (1991). Seismotectonics of the Portland, Oregon, region, *Bull. Seism. Soc. Am.* **81,** 109–130.

Yelin, T. (1992). An earthquake swarm in the north Portland (Oregon) Hills: more speculations on the seismotectonics of the Portland Basin (abstracts with programs), *Geol. Soc. Am.* **24,** 92.

Zollweg, J. E. and R. S. Crosson (1981). The Goat Rocks Wilderness, Washington earthquake of 28 May 1981 (abstract), *EOS* **62,** 966.

University of Washington
Geophysics
Box 351650
Seattle, Washington 98195-1650
(G.C.T., R.S.C.)

U.S. Geological Survey
Box 25046
Federal Center
Denver, Colorado 80225-0046
(D.L.C.)

U.S. Geological Survey
University of Washington
Geophysics
Box 351650
Seattle, Washington 98195-1650
(T.S.Y.)

Manuscript received 20 July 1995.